Performance Comparison of Using Shunt-Based and Integrated Current Sensing for Sensorless Field-Oriented Control

John Emmanuel Tan | Power Integrations, Philippines

Abstract

Sensorless Field-Oriented Control (FOC) for 3-phase Permanent Magnet Synchronous Motors (PMSM) requires motor phase current information. This paper compares the performance of shunt-based and low-side switch integrated current sensing in terms of system efficiency and ease of use for predictive maintenance. The use of integrated current sensing in the low-side switch along with a current reconstruction algorithm doubles the information resolution and reduces the number of required components. Predictive maintenance techniques use sensed information to infer the health of the system. Integrated current sensing provides more information and better noise immunity, resulting in enhanced system performance and easier use for predictive maintenance analysis.

1 Introduction

Sensorless Field-Oriented Control (FOC) of three-phase motors makes use of phase current information [1,2]. This paper examines the performance of two current sensing methods: shunt-based and low-side switch-integrated sensing [3,4]. For shunt-based sensing, signal conditioning circuits are required to add offset and amplification to the sense signal. In contrast, integrated current sensing reduces the number of discrete components, including the current shunt resistors, which dissipate energy and are more expensive than the two small-signal resistors used in an integrated approach. However, with inte-grated current sensing, only the negative motor phase current is sensed, necessitating the implementation of a reconstruction algorithm to create the phase-current waveform for an entire cycle [5].

The current information can also be used for protection and to gain insights into early motor degradation, which may then be addressed through predictive maintenance [6,7]. Two approaches for predictive maintenance are explored in this paper: Park Circle [6,8], and Motor Current Signal Analysis (MCSA) [9]. The Park Circle is performed by plotting the Alpha and Beta phase-currents on an XY plot. Ideally, the plot should form a perfect circle. Deviations from this shape may suggest abnormal conditions or asymmetric operation. MCSA is performed using Fast Fourier Transform (FFT) to compare the signature of the motor phase-current with and without fault conditions. The features extracted from the current signature are then used to develop a Random Forest (RF) classifier model to determine if the motor is “healthy” or “faulty.”

This paper will describe the FOC algorithm in Section 2 to determine where the current information is used. Section 3 will discuss how the current information is sensed. Section 4 explores how predictive maintenance can be implemented using the sensed current information. Finally, the experimental results of the study are discussed in Section 5.

2 Field-Oriented Control

FOC is performed by controlling the stator current vector components, namely the flux- and torque-producing components [1,2]. For Permanent Magnet Synchronous Motors (PMSM), the flux-producing component of the stator current vector is normally adjusted to zero since the flux is provided by the permanent magnets in the rotor. This maximizes the torque produced by the motor.

This method of control requires knowledge of rotor position and stator current measurement. The FOC block diagram is illustrated in **Figure 1**.

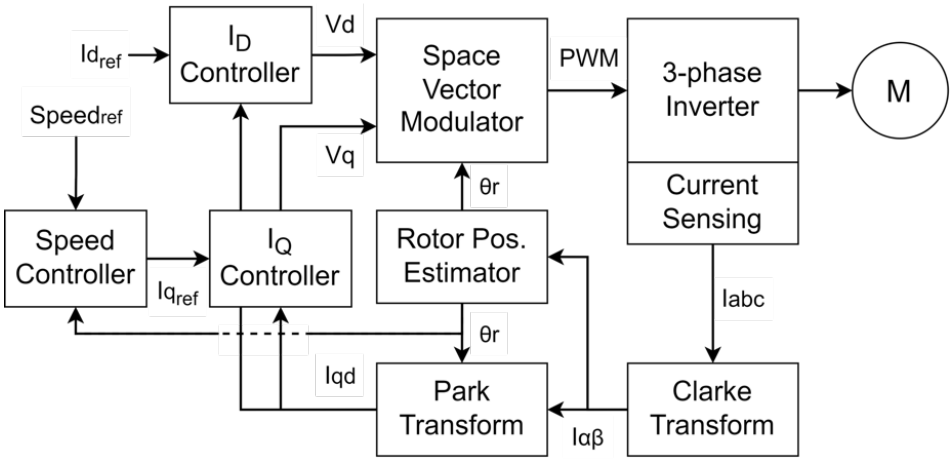

Figure 1 Field-oriented control block diagram.

2.1 Rotor Position

The position of the rotor during operation is used by the control system to provide the appropriate control signals. Sensors, such as rotary encoders, can easily be used to determine this rotor position. However, integrating such sensors adds extra cost and introduces reliability concerns.

2.1.1 Rotor/PM Flux Estimation

Sensorless control schemes, such as the rotor flux observer method, are used in place of the position sensor. In the rotor flux observer method, the motor model equation in Eq. (1) is used.

$$V = iR + L\frac{di}{dt} + e \qquad (1)$$

$$e = V - iR - L\frac{di}{dt} = \frac{d\Psi_{PM}}{dt}$$

$$\Psi_{PM} = \int e\,dt = \int (V - iR)dt - Li \qquad (2)$$

$$\Psi_S = \int \left(V - iR - V_{comp}\right)dt$$

$$V_{comp} = \left(k_p + \frac{k_i}{s}\right) \cdot \Psi_S$$

$$\Psi_{PM} = \int \left(V - iR - V_{comp}\right)dt - Li \qquad (3)$$

where: V is the applied voltage across the winding, i is the winding current, R is the winding re-sistance, L is the winding inductance, e is the Motor back-electromotive force or back-EMF, Ψ_{PM} is the flux of the rotor permanent magnet, Ψ_S is the stator flux, V_{COMP} is the DC offset compensator, while the k_p and k_i are the PI correction feedback gains.

Equation (2) describes the rotor or permanent magnet (PM) flux estimation. A DC offset drift is observed when ideal integrators are used as parameters and measurement inaccuracies are accumulated by the integrator. To mitigate these effects, Proportional-Integral (PI) correction feedback, V_{comp}, is used for compensation [1,2].

Figure 2 shows the structure used for estimating the rotor/PM flux as described by Eq. (3). Motor parameters such as Stator Resistance, R, and Stator Inductance, L, are used. The Applied Voltage, V, and Motor Phase Current, i, serve as in-puts to the estimator block.

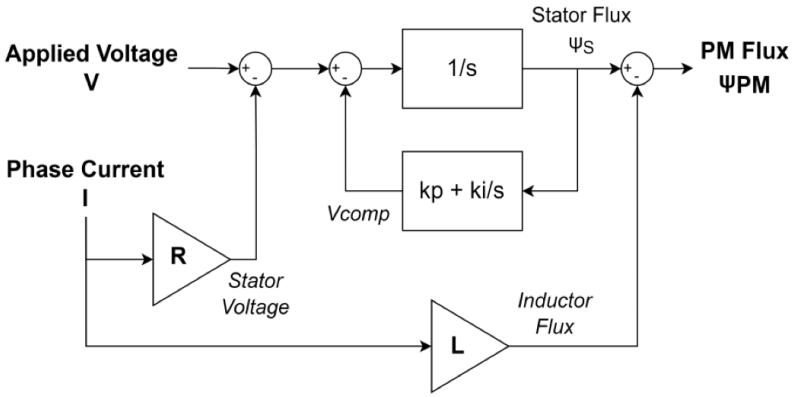

Figure 2 Rotor/PM flux estimation.

2.1.2 Rotor Position Estimation

The estimation for the rotor position (θ) can be simplified by transforming the 3-phase reference frame (U-, V-, and W- axes) into the stationary 2-phase reference frame (α-, β- axes), see **Figure 3**.

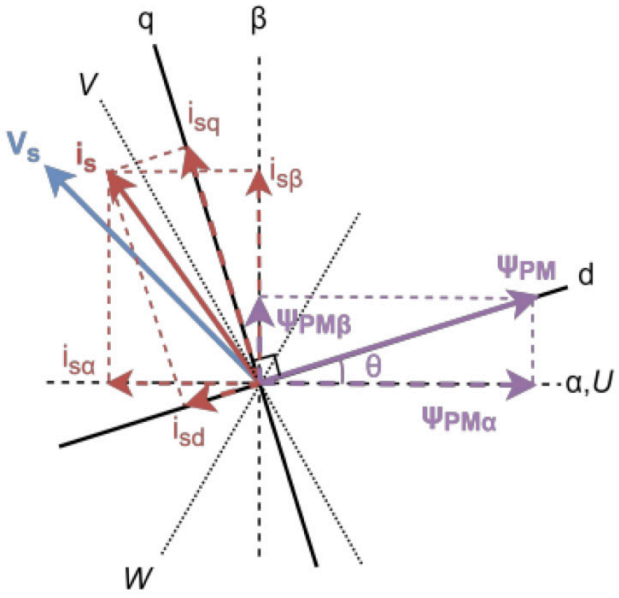

Figure 3 Motor control space vector diagram

Equation (4) provides the translation of a 3- to 2-phase reference frame, known as the Clarke Transform. After transforming the stator current information into the stationary reference frame components $i_{s\alpha}$ and $i_{s\beta}$, they are used as inputs to the rotor flux estimator shown in **Figure 2**.

$$\begin{bmatrix} i_\alpha \\ i_\beta \end{bmatrix} = \begin{bmatrix} 1 & 0 & 0 \\ \frac{\sqrt{3}}{3} & \frac{2\sqrt{3}}{3} & 0 \end{bmatrix} \begin{bmatrix} i_U \\ i_V \\ i_W \end{bmatrix} \quad (4)$$

$$\begin{bmatrix} i_q \\ i_d \end{bmatrix} = \begin{bmatrix} -\sin\theta & \cos\theta \\ \cos\theta & \sin\theta \end{bmatrix} \begin{bmatrix} i_\alpha \\ i_\beta \end{bmatrix} \quad (5)$$

where: i_α and i_β are the stator current components in the stationary reference frame, iU, iV, and iW are the stator current components in the 3-phase windings, while i_q and i_d are the stator current components in the synchronous reference frame.

The rotor flux components estimated in the stationary reference frame, $\Psi_{PM\alpha}$, and $\Psi_{PM\beta}$, are then used to estimate the rotor position [2]. The examination confirms that the trigonometric function arctangent is usable, albeit with additional filtering in the form of a Phase-Locked Loop (PLL) structure. Similarly, the Quadrature PLL or Q-PLL shown in **Figure 4** can also be used to achieve the same angle calculation and noise filtering functionality.

2.2 Current Control

The stator current can further be analyzed and broken down into its flux- and torque- producing components using the Park Transform described in Eq. (5). By using the estimated rotor position (θ) as the input to the transformation, the translated horizontal axis (Direct or d- axis) is parallel to the rotor position, while the translated vertical axis (Quadrature or q- axis) is perpendicular to the rotor position. This is also known as the synchronous or rotating reference frame since it rotates with the rotor.

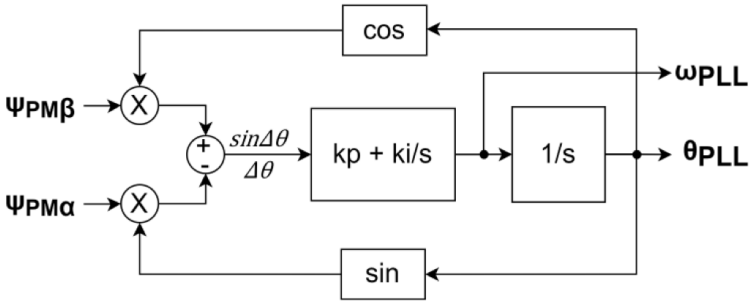

Figure 4 Quadrature phase-locked loop structure.

The stator current component parallel to the rotor, or the Direct Current (I_D) is referred to as the flux- producing current; while the component perpendicular to the rotor, or the Quadrature Current (I_Q) is known as the torque-producing current.

I_Q and I_D control are both implemented in FOC, as shown in **Figure 1**. Typically, I_D is reduced to zero since the flux is already provided by the rotor permanent magnets. A special control technique called Flux Weakening can reduce I_D to a nega-tive value to increase the motor operating speed at the expense of reduced torque. I_Q is used to indirectly regulate the output torque, such that for Speed Control operation, the target I_Q is provided by the Speed Controller to reach the target speed.

The Quadrature and Direct Currents are DC values since they are in the synchronous reference frame. Proportional-Integral (PI) controllers are now suitable for regulating these components.

The Space Vector Modulator applies the appropriate stator voltage vector by providing the Pulse-Width Modulated signals to the inverter. The modulator takes the target Quadrature and Direct Voltages (V_Q and V_D) as inputs, see **Figure 1**. The magnitude and angle of the applied vector vary depending on the output of the current controllers which is finite until the torque is maximized (when ID becomes zero).

3 Current Sensing

In FOC, the stator current information is used for rotor position estimation and stator current component control.

Various current sensing methods are available, such as different current sensors [3, 4]. In this paper, current-shunt based sensing and low-side switch integrated current sensing is scrutinized.

Current shunt-based sensing requires a resistive element placed on the path of the current to be sensed. The voltage across the resistive element is measured to determine the shunt current. This sensed voltage is processed by a signal pre-processing circuit then fed into an Analog-to-Digital Converter (ADC) used by the motor controller.

3.1 Shunt-Based Current Sensing Schemes

Figure 5 illustrates the different locations in the inverter and motor where the phase current information can be sensed [3]: 1) High-side DC-bus current sensing, 2) Motor in-line current sensing, 3) Low-side inverter leg current Sensing, and 4) Low-side DC-bus current sensing.

High-side current sensing techniques, such as high-side DC-bus sensing and motor in-line sensing, require differential sensing since it is riding on a high-voltage signal. The additional challenge of resolving a millivolt level signal combined with the high-voltage signal containing fast dv/dt needs to be resolved.

Conversely, low-side current sensing techniques, such as low-side DC-bus sensing and low-side inverter leg current sensing, are already referenced to the ground, allowing simpler sensing methods. In low-side inverter leg current sensing, the sensed information is a negative representation of the actual current since sensing is performed adjacent to the low-side switch.

For DC-bus current sensing — both high-side and low-side — an additional reconstruction algorithm is required to determine the 3-phase motor currents. This current reconstruction requires more complex ADC sampling.

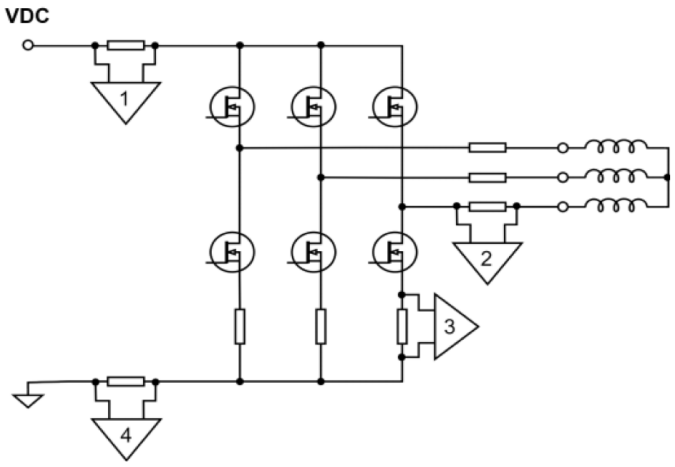

Figure 5 Inverter current sensing schemes.

3.1.1 Shunt-Based Sensing in the Low-Side Inverter Leg

Low-side shunt-based sensing increases the power dissipation of the system as it is placed along the high-current path. This reduces the advantage of using a low-channel resistance switch. To limit the dissipation, the shunt resistance is minimized.

Before feeding the sense current signal to the controller ADC, a signal processing circuit is necessary. Amplification is required to increase the magnitude of the sense signal which is very low due to the need for minimum sense resistance. Additionally, a DC offset is required to account for the negative current passing through the shunt. **Figure 6** shows the signal processing circuit required for all three phases.

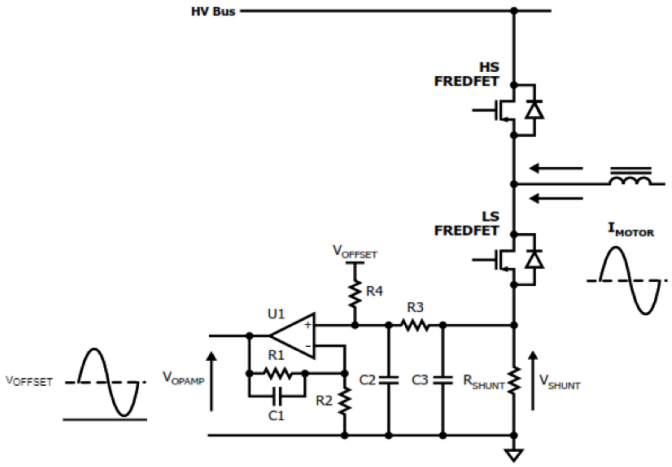

Figure 6 Low-side switch shunt-based sensing.

The sampled ADC signal is processed by the controller by removing the offset and reversing the amplification gain to calculate the actual motor phase current.

Both positive and negative current information must be represented in the sensed signal to be sampled by the ADC.

3.2 Integrated Current Sensing in the Low-Side Switch

Current sensing can also be integrated into the power switches to reduce the need for external resistive sensing elements. **Figure 6** shows lossless current sensing integrated using a parallel sensing transistor. This sensing transistor outputs a current proportional to the current passing through the main power transistor (see **Figure 7**).

An amplifier is also integrated to increase the magnitude of this sense current signal. An inexpensive small-signal resistor is used to convert this sense current to a voltage signal captured by the ADC.

Only half of the current information is sensed since the current only passes through the sensing transistor when the power switch is on. An additional current reconstruction algorithm [5] is required to reproduce the missing information for correct FOC operation.

As the current vector rotates, the available sensed current information alternates between highlighted and non-highlighted sectors in **Figure 8**. In the highlighted sectors current information is available for one phase; in the non-highlighted phases, current from 2 phases is known.

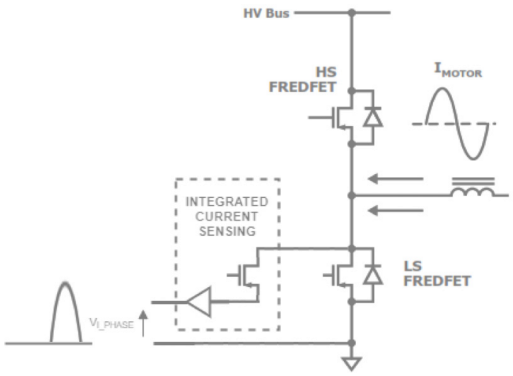

Figure 7 Low-side switch integrated sensing.

3.2.1 Current Reconstruction

As outlined at an IAS conference [5], the feasibility of using the integrated current sensor and the processing required to use the current information must be determined.

If current information is available for two phases (non-highlighted sectors, e.g., i_b and i_c), the third phase current (e.g., i_a) is reconstructed using Eq. (6). If current information is only available for one phase (highlighted sectors, e.g., i_c), the second and third phase currents (e.g., i_a^* and i_b^*) are reconstructed using Eq. (7), (8), and (9) depending on which two are applicable. The current vector angle, $\theta_{\alpha\beta}$, is required for the reconstruction.

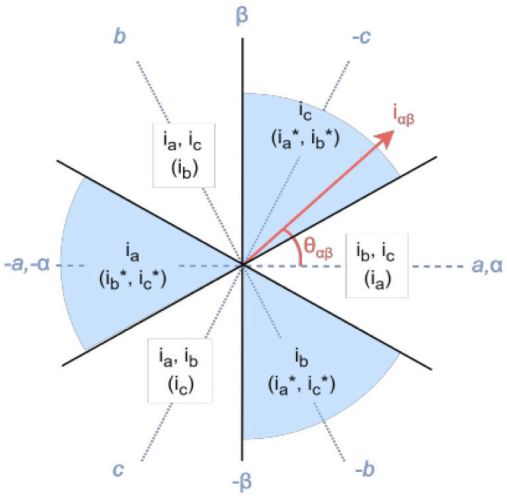

Figure 8 Current reconstruction diagram.

$$i_a + i_b + i_c = 0 \quad (6)$$

$$i_a = i_{mag} \cos \theta_{\alpha\beta} \quad (7)$$

$$i_b = i_{mag} \cos(\theta_{\alpha\beta} - 120°) \quad (8)$$

$$i_c = i_{mag} \cos(\theta_{\alpha\beta} + 120°) \quad (9)$$

where: i_a, i_b, and i_c are the stator current components in the 3-phase windings (to be used interchangeably with i_U, i_V, and i_W), i_{mag} is the stator current magnitude, while $\theta_{\alpha\beta}$ is the current vector angle.

Since only negative current information needs to be represented in the sensed signal to be sampled by the ADC, and the positive current information is reconstructed based on the algorithm, the available information resolution is twice that of shunt-based sensing.

4 Predictive Maintenance

Predictive maintenance techniques used in inferring the health of induction motors have been extensively explored [6,7]. These methods are also applicable for PMSM.

Table 9 describes common methods for performing predictive maintenance on different motor control subsystems and their significance for fault detection. The following predictive maintenance techniques have been listed: Extended Park Vector Approach (EPVA), Motor Current Signature Analysis (MCSA), and Instantaneous Power Signature Analysis (IPSA). These techniques are also known as Electrical Signature Analysis (ESA). ESA is a non-invasive method since no added sensors are required. Instead, it is performed on the sensed voltage and current information, which may already be used for control.

This paper focuses on techniques that utilize sensed current information. Mechanical imbalance and misalignment are simulated and compared with normal operation to provide comparative performance data.

4.1 Park Vector Approach

For steady-state FOC operation with constant torque, the phase current vector rotates at a constant magnitude. The representation of the phase current vector varies depending on the reference frames discussed in the FOC section.

Subsystem	Method	Significance
Supply	Power Quality	High
	EPVA (Voltage)	Medium
Mechanical	MCSA	High

Imbalance or Misalignment	Vibration	High
	EPVA	Medium
Insulation Faults	Partial Discharge	High
	EPVA	Low
Stator Electrical Imbalance	EPVA	High
	MCSA	Medium
	Power Quality	Medium
Bearing Faults	Vibration	High
	Wavelet on Current	Medium
	MCSA, EPVA and IPSA	Low
Coupling and Load Mechanical Failures	Vibration	High
	MCSA, EPVA and IPSA	Medium

Table 1 Predictive maintenance techniques for different motor subsystems.

In the stationary reference frame, the phase current components, $i_{s\alpha}$ and $i_{s\beta}$, are sinusoidal in nature. Plotting these components in an XY plot yields a circular graph for a healthy system [8].

In contrast, in the synchronous reference frame, the phase current components, i_{sq} and i_{sd}, are DC in nature. Plotting these components in a polar graph using the estimated rotor position as the angle also yields a circular graph for a healthy system.

Deviation from the ideal circular shape denotes issues in the balance of the 3-phase current which can be identified by analyzing the images.

4.2 Motor Current Signature Analysis

Further analysis can be performed with the stator current information by using transformation tools to extract the signal signature or features [6, 9].

Fast-Fourier Transform (FFT) is a technique used to extract signal features. FFT extracts the magnitude of the signal components across the frequency spectrum. These features are further processed to determine the health of the system.

5 Experimental Results

For this paper, sensorless FOC is used to drive a 300 W 3-phase motor capable of running up to 5000 RPM at a control-loop frequency of 8 kHz. For the inverter, the Power Integrations Reference Design Kit RDK-853 is used. This inverter makes use of the integrated half-bridge driver BridgeSwitch™ BRD1265C, which features an integrated lossless current mirror (IPH) to provide motor current information. The controller used is the 32-bit Arm® Cortex®-M0 XMC1400, a low-cost microcontroller from Infineon. The control code library utilized is the MotorXpert™ Suite from Power Integrations, which supports both shunt-based and integrated current sensing operation.

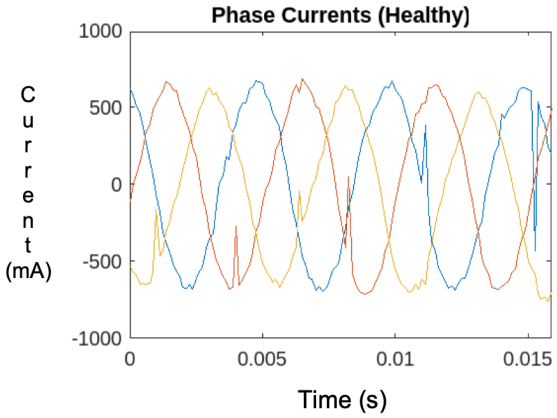

Figure 9 Current information with shunt-based sensing.

5.1 Current Information

The motor was operated at 3000 RPM for both shunt-based and integrated current sensing schemes. **Figures 9** and **10** show the current information used by the FOC operation for both schemes. Noticeably, the current information in **Figure 9** had more noise compared to **Figure 10**.

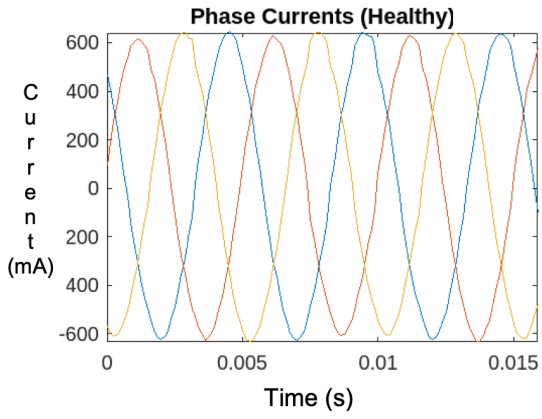

Figure 10 Current information with integrated sensing.

5.2 Motor Drive System Efficiency

Figure 10 shows the visualization for how the mo-tor drive system efficiency was calculated.

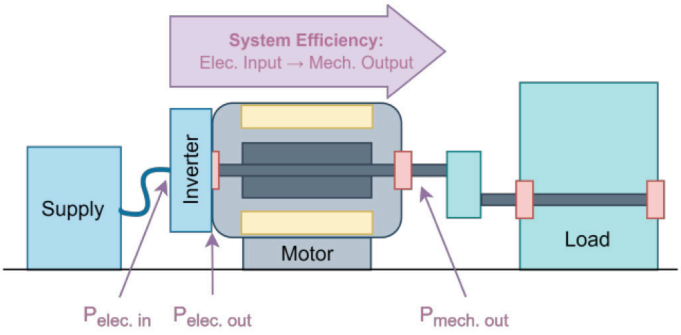

Figure 11 Motor drive system efficiency.

For the measurement of this performance, the motor output torque was regulated at 0.45 Nm and the speed maintained at 3000, 4000, and 4500 RPM. The input electrical power was measured at the input of the inverter, while the mechanical output power was calculated using Eq. (10). The system efficiency was calculated using Eq. (11). The results are shown in **Tables 2** and **3**.

$$P_{mech\_out} = \tau \cdot \omega \qquad (10)$$

$$\eta_{system} = \frac{P_{mech\_out}}{P_{elec\_in}} \times 100\% \qquad (11)$$

where: P_{mech_out} is the output mechanical power, τ is the torque, ω is the angular speed, P_{elec_in} is the input electric power, and η_{system} is the system efficiency.

Table 4 shows the improvement in system performance using the integrated current sensing scheme. Across the three conditions recorded, the average reduction in wasted power was ~1.03 W when integrated current sensing was used.

The measured improvement was higher than just the loss dissipated by the shunt resistors. Better signal quality of the current information due to the increased resolution and lower noise contributed to the system efficiency improvement by optimizing the FOC operation such that lower electrical input power was required to provide the same mechanical power output.

Speed (RPM)	Mechanical Output Power (W)	Input Electrical Power (W)	System Efficiency (%)
3000	142.2	176.8	80.43
4000	189.7	230.4	82.34
4500	211.9	255.5	82.94

Table 2 System efficiency for shunt-based sensing.

Speed (RPM)	Mechanical Output Power (W)	Input Electrical Power (W)	System Efficiency (%)
3000	142.2	175.3	81.18
4000	189.7	229.6	82.62
4500	211.9	254.7	83.20

Table 3 System efficiency for integrated sensing.

Speed (RPM)	Input Electrical Power Delta (W)	System Efficiency Delta (%)
3000	– 1.5	+0.75
4000	– 0.8	+0.28
4500	– 0.8	+0.26

Table 4 System efficiency improvement between shunt-based and integrated sensing.

5.3 Predictive Maintenance — Park Vector Approach

The current information in **Figures 9** and **10** is from the operation of a properly mounted motor. To simulate a mechanical imbalance or misalignment fault, mounting supports were intentionally loosened. Based on **Table 1**, EPVA had a Medium Significance while MCSA had a High Significance in detecting this fault condition.

Figures 12 and **13** show the Park Circle visualization for healthy and faulty operation, respectively, for a motor with shunt-based sensing. It is difficult to determine which condition is faulty due to the spikes in the Park Circle caused by the noise in the sampled current information.

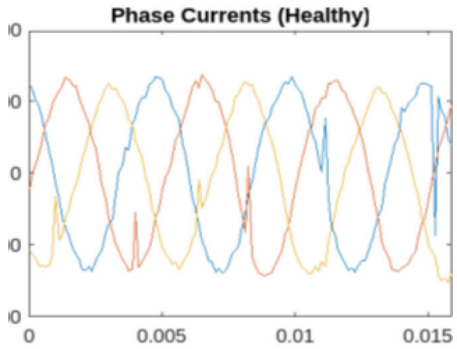

Figure 12 Park Circle with shunt-based current sensing for a healthy system.

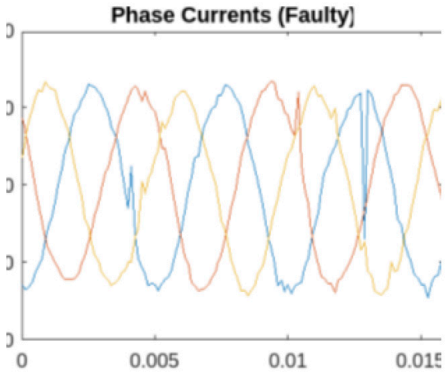

Figure 13 Park Circle with shunt-based current sensing for a faulty system simulation.

Figures 14 and **15** show the Park Circle visualization for healthy and faulty operation respectively for a motor employing Integrated current sensing. The waveform in **Figure 15** has a more noticeable bulge from the 330 ° to 30 ° part of the circle.

The integrated current sensing scheme enables easier analysis of Park Circle due to the better signal quality.

5.4 Predictive Maintenance – Motor Current Signal Analysis

MCSA is applied to the current information by using FFT to extract the features.

Figures 16 and **17** show the current signature from shunt-based sensing during healthy and faulty operation, respectively. The magnitude of the 0 Hz component can be interpreted as the magnitude of the current vector. The signature during faulty condition shows more peaks compared to the signature for healthy operation.

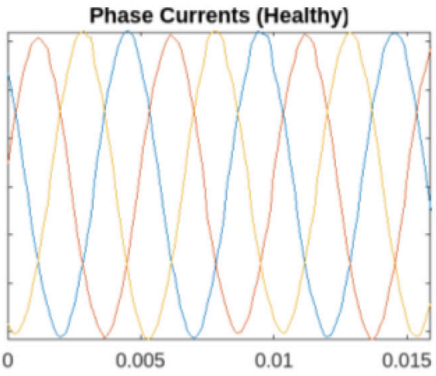

Figure 14 Park Circle with integrated current sensing for a healthy system.

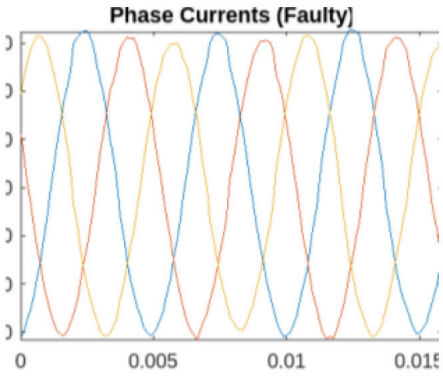

Figure 15 Park Circle with integrated current sensing for a faulty system simulation.

Figures 18 and **19** show the current information signature from integrated sensing during healthy and faulty operations, respectively. Similarly, the magnitude of the 0 Hz component can be interpreted as the magnitude of the current vector. The magnitude during the faulty condition is higher (626.2) compared to that of the healthy condition (607.9). This means that a higher current is required to drive the motor when supporting the same load and speed.

Furthermore, the feature at 93 Hz which is closest to the motor speed in terms of rotation frequency, is also highlighted by these signatures. For integrated current sensing, a higher magnitude is observed for the faulty operation (21.20) compared to the healthy operation (7.07) and suggests that the signal has 3x the magnitude at that frequency.

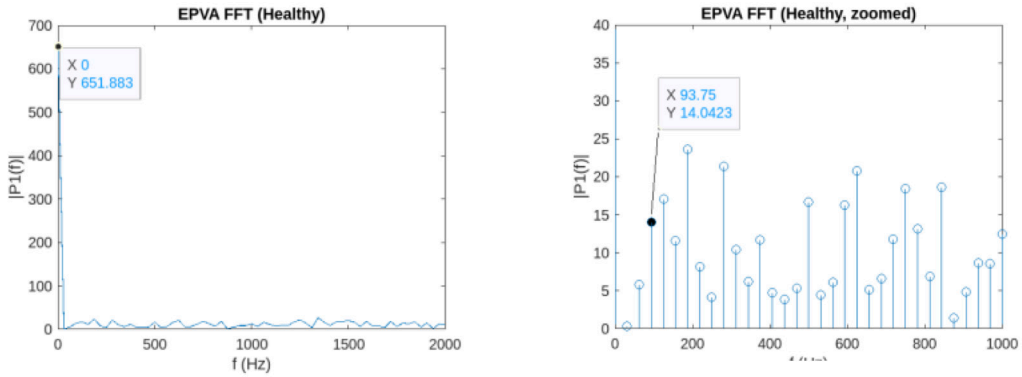

Figure 16 Motor current signature analysis with shunt-based current sensing for a healthy system.

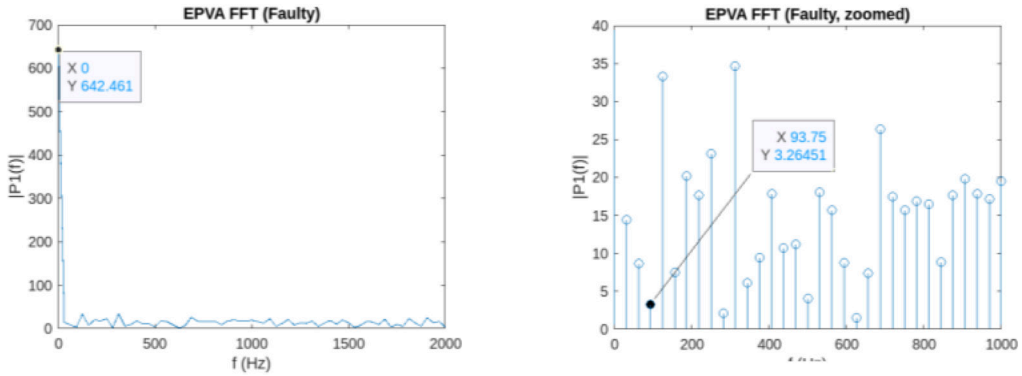

Figure 17 Motor current signature analysis with shunt-based current sensing for a faulty system simulation.

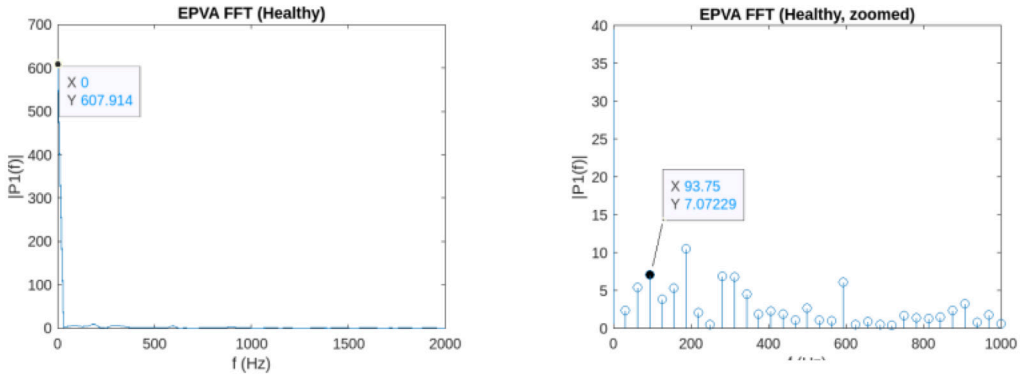

Figure 18 Motor current signature analysis with integrated current sensing for a healthy system.

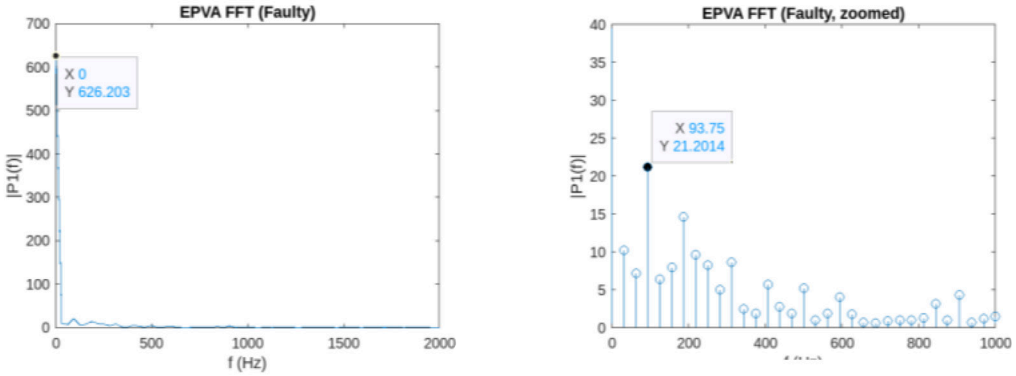

Figure 19 MCSA with integrated current sensing for a faulty system simulation.

A method of classification is required to take advantage of these extracted signatures and determine the health of the system.

5.4.1 Random Forest Classification

The motor was run at 3000 RPM for both healthy and faulty conditions. Data was captured and split into training and test data. MCSA was applied to the current data, and the extracted features used to train a Random Forest (RF) classification model that was then verified using the test data [10, 11].

A trained RF classifier is composed of decision trees, which are also called estimators. The final classification (i.e., “Healthy” or “Faulty”) is determined by a majority vote from the estimators.

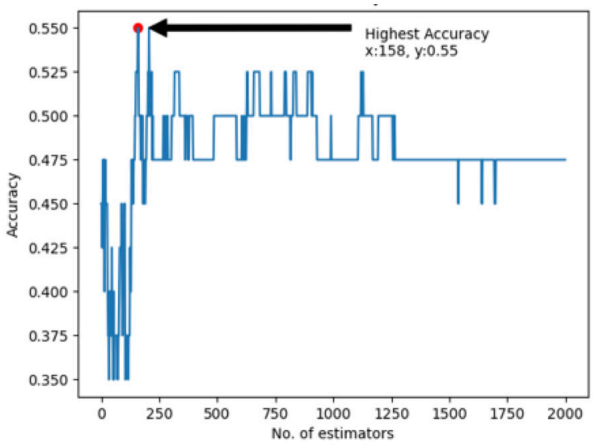

Figure 20 RF classifier testing with current information from shunt-based sensing.

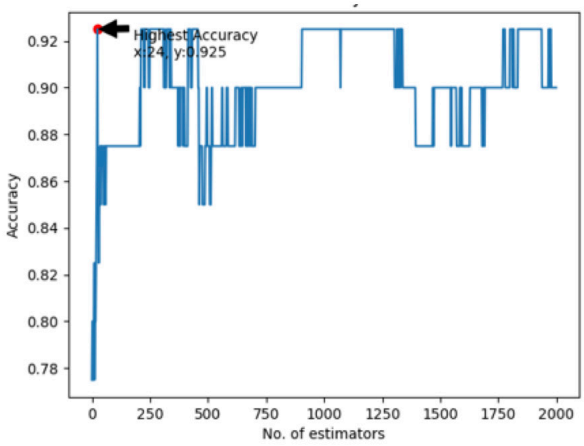

Figure 21 RF classifier testing with current information from integrated sensing.

The model has been developed and tested after iterating with the number of estimators (up to 2000). The accuracy compared with the number of estimators was graphed and shown in **Figures 20** and **21**. For shunt-based sensing, the maximum accuracy achieved was 55% with 158 estimators, while for integrated sensing, the maximum accuracy was 92.5% with 24 estimators.

This result showed that due to the better quality of the current information, developing more accurate predictive maintenance models is easier with integrated sensing compared to shunt-based sensing.

Conclusion

In this paper, the performance of shunt-based and integrated current sensing was compared in terms of system efficiency and compatibility with predictive maintenance techniques.

FOC was explored to describe where the current information is mainly used — rotor position estimation and current control. The different current sensing techniques were also discussed to give an overview of shunt-based and integrated sensing.

An improvement in the system efficiency was observed due to the increased resolution and better quality of the current information. Further study is recommended to determine if the removal of the resistive element between the low-side switch and the ground has more impact on metrics of performance beyond system efficiency.

The better quality of current information also helps in the development and implementation of predictive maintenance systems. Two methods of analysis were explored: Park Vector approach, and MCSA, both confirming easier analysis when integrated sensing was used compared to shunt-based sensing. The features extracted with MCSA were also used to develop an RF classifier. The model developed with integrated sensing was more accurate with fewer estimators compared to when the model was developed with shunt-based sensing. Further study was recommended to confirm the findings with different predictive maintenance techniques.

References

[1] Shen J, Hao H, Wang C, Jin M. 2013. Sensorless control of IPMSM using rotor flux observer. COMPEL - The international journal for computation and mathematics in electrical and electronic engineering. Vol. 32 No. 1, pp. 166-181.

[2] Sreepriya R, Rajagopal R. Sensorless control of three phase BLDC motor drive with improved flux observer. 2013 International Conference on Control Communication and Computing (ICCC). India, 2013. pp. 292-297.

[3] Persson E. Motor current measurement using time-modulated signals. Proceedings of the Power Conversion Conference-Osaka 2002 (Cat. No.02TH8579). Japan. 2002. pp. 716-720 vol.2.

[4] Patel A, Ferdowsi M. Current Sensing for Automotive Electronics—A Survey. IEEE Transactions on Vehicular Technology. vol. 58, no. 8, pp. 4108-4119. 2009.

[5] Chakrabarti S, Jahns T M, Lorenz R D. A current reconstruction algorithm for three-phase inverters using integrated current sen-sors in the low-side switches. 38th IAS Annual Meeting on Conference Record of the Industry Applications Conference. 2003. USA. 2003. pp. 925-932 vol.2.

[6] Bonaldi E L, de Oliveira L E L, Borges da Silva J G, Lambert-Torres G, Borges da Silva L E. 2012. Predictive Maintenance by Electrical Signature Analysis to Induction Motors. In: R. Araujo, Ed., Induction Motor Modelling and Control. InTech, Croacia, 487-520.

[7] Siddiqui K, Sahay K, Giri V, Scholar P. Health monitoring and fault diagnosis in induction motor-a review. International Journal of Advanced Research in Electrical, Electronics and Instrumentation Engineering. 2014. 3: 6549–65.

[8] Boudiaf M, Cherroun L, Benbrika M. 2018. Real-time diagnosis of three-phase induction machine using Arduino-Uno card based on park's circle method. Diagnostyka. pp. 19(3), 63-71.

[9] Bouslimani S, Drid S, Chrifi-Alaoui L, Bussy P, Ouriagli M, Delahoche L. An extended Park's vector approach to detect broken bars faults in Induction Motor. 2014 15th International Conference on Sciences and Techniques of Automatic Control and Computer Engineering (STA), Tunisia. 2014. pp. 411-416.

[10] Prihatno A T, Nurcahyanto H, Jang Y M, Predictive Maintenance of Relative Humidity Us-ing Random Forest Method. 2021 International Conference on Artificial Intelligence in In-formation and Communication (ICAIIC). Korea (South). 2021. pp. 497-499.

[11] Taşcı B, Omar A, Ayvaz S. 2023. Remaining useful lifetime prediction for predictive maintenance in manufacturing. Computers & Industrial Engineering. Volume 184, Article 109566.

For more information,
visit **power.com**™

power integrations

061024